Thermocapillary instability in an evaporating two-dimensional thin layer film

Andriy A. Avramenko, Igor V. Shevchuk, Souad Harmand, Andrii I. Tyrinov

International Journal of Heat and Mass Transfer 91 (2015) 77–88

Thermocapillary instability in an evaporating two dimensional thin layer film

Andriy A. Avramenko [a], Igor V. Shevchuk [b], Souad Harmand [c,d,*], Andrii I. Tyrinov [a]

[a] Institute of Engineering Thermophysics, National Academy of Sciences, Kiev 03057, Ukraine
[b] MBtech Group GmbH & Co. KGaA, 70736 Fellbach-Schmiden, Germany
[c] Université de Lille Nord de France, F-59000 Lille, France
[d] UVHC, TEMPO/DF2T, Valenciennes 59313, France

Keywords:
Heat transfer
Boiling
Thermocapillary instability
Marangoni number
Capillary number

A B S T R A C T

A novel two-dimensional model for the thermocapillary instability of a thin liquid film was developed and validated in the paper. The model incorporates a novel solution for the unperturbed velocity components and the thin film thickness (based on the boundary layer approach and balance equation) subject to evaporation under the boundary conditions of either mechanical interaction between the liquid and vapor phases or stationary vapor above the interphase boundary. A novel model for thermocapillary instability in a thin film was developed in frames of the linear perturbation method, i.e. modified Orr–Sommerfeld equation, taking into account the surface and London–van der Waals forces. The critical Reynolds number was computed by considering the two-dimensional disturbances, which according to the Squire's theorem are more dangerous than the three-dimensional disturbances. For constant surface tension at the interphase interface, the unperturbed velocity profile is parabolic, and maximum increases, while the critical Reynolds number decreases with the decreasing capillary number. If the surface tension at the interphase interface depends on the temperature, the maximum of the undisturbed velocity profile increases with the decreasing capillary number and increasing modified Marangoni number, which entails more rapid decrease in the critical Reynolds number. It was also shown that the flow is destabilized by the increase in the temperature difference between the wall and the vapor, by the decrease in the absolute pressure and by the increase in the thermal conductivity. To confirm existence of different flow regimes in the nanofluid film, numerical simulations of capillary flow was performed, which exhibit qualitative consistence with the stability theory.

1. Introduction

The constant demand for more powerful and smaller device dimensions in many industrial sectors, including transportation, energy supply and production and electronics, raised heating or cooling fluids properties to the rank of ones of the major parameters taken into consideration in designing and controlling such devices.

Among those properties is the heat and mass transfer phenomena at the two-phase interface of evaporating meniscus in capillary flows witch make much influence on the overall performance of the process.

An example of a heat and mass transfer device where three phase contact line evaporation occurs are the heat pipes and vapor chambers. Contrary to the conventional "normal-size" heat pipe, a micro heat pipe does not incorporate a wick structure. Instead, a micro heat pipe makes use of the capillary pressure that arises due to the sharp-angle corners and forces the condensate to circulate back to the evaporator region [1]. Heat pipes are relatively widely used for cooling purposes in the transport, aerospace and other applications. A recent review paper [2] provides a number of the examples of such applications [2]. Quite many studies have been undertaken in order to develop modeling approaches to predictions of the thermal performance of micro heat pipes [1,3–5]. Anyway, a deeper understanding of the evaporation processes in the micro-region is still to be gained in order to develop physically adequate and accurate methods of simulations and thermal design.

For some complex two-phase heat transfer phenomena, the detection of triple line is very important for determining the dry area.

The problem of the evaporation of a liquid along a contact line recently attracted the interest of many researchers in many industrial applications. Many researches are concentrated on natural

* Corresponding author at: Université de Lille Nord de France, F-59000 Lille, France.

DOI : 10.1016/j.ijheatmasstransfer.2015.07.063

Nomenclature

c	specific heat capacity
Ca^*	modified capillary number, Eq. (22)
G	flow rate per unit length, Eq. (34)
Δh	latent heat of evaporation
k	thermal conductivity
K	curvature
$\dot{m}$	(outward) evaporative mass flux crossing the interface
M	non-dimensional parameter, Eq. (41)
Ma	Marangoni number, Eq. (28)
Ma^*	modified Marangoni number, Eq. (27)
Ma^{**}	modified Marangoni number, Eq. (45)
n	the normal to the interface, Eq. (14)
p	pressure
Pe	Peclet number, Eq. (29)
Re	Reynolds number, Eq. (74)
S	non-dimensional parameter, Eq. (41)
T	temperature
T_υ	vapor temperature,
T_w	wall temperature (reference temperature)
t	time
u	streamwise velocity component (x-component)
U	dimensionless velocity, Eq. (20)
υ	transverse velocity component (y-component)
W	dimensionless velocity, Eq. (21)
x, y, z	Cartesian coordinates

Greek symbols

γ	the surface tension gradient with respect to temperature, Eq. (9)
δ	film thickness
δ_0	initial film thickness
ΔT	temperature difference across the film, Eq. (17)
η	dimensionless coordinate, Eq. (19)
κ	parameter, Eq. (30)
Θ	dimensionless temperature, Eq. (17)
μ	dynamic viscosity
ρ	density
σ	interface surface tension
τ	boundary stress friction
ξ	dimensionless coordinate, Eq. (31)

Subscripts

0	unperturbed (basic flow) parameters
f'	perturbed value oft he function f
cap	capillary
cr	critical value, Eq. (98)
disj	disjoining
w	wall

Acronyms

2D	two-dimensional

evaporation at ambient temperature, but the study of coupled heat and mass transfer problem when the substrate is heated is also important for understanding the heat transfer enhancement as well as contact line dynamics.

Modelling of heat and mass transfer in micro heat pipes is based on the knowledge of the flow regime conditions. Onset of instabilities, beginning and end of the laminar-turbulent transition is subject to physical effects of the processes in micro heat pipes, which are rather different from those macrochannels. Boiling, evaporation and capillary effects are additional factors, which complicate the models to be used.

As for today, one can mention quite many publications where different types of the thermocapillary instability were studied theoretically. They differ by different approaches and applicability of their results. In the works [6,7], the instability was investigated using a non-linear approach with 3D perturbations imposed on the main flow. This approach resulted in the equations of the Orr–Sommerfeld type studied to find eigenvalues. Stability analysis of Poiseuille–Benard–Marangoni flow was performed in the work [6] as applied to a horizontal infinite liquid film that flows in one direction and is uniformly heated from below. Two limiting cases were studied here: pure buoyancy effect (Ma = 0) and pure thermocapillary effect (Ra = 0). As shown in the work [6], critical Marangoni number and critical Rayleigh number are functions of the Biot, Reynolds and Prandtl numbers. The work [7] concerns with the linear instability analysis of thermocapillary convection in a system with two immiscible liquids separated by an interface and a constant horizontal temperature gradient set on the interfaces. Two types of the instabilities were imposed: (a) streamwise homogeneous perturbations with zero wave number; (b) spanwise homogeneous perturbations with zero wave number. In the case (a), convection took place in the stationary or oscillatory mode, whereas in the case (b) convection arose in the oscillatory mode as a traveling wave that spread in the direction of the main flow. Effects of the Biot number on the unstable modes were also studied.

A classical linear approach to thermocapillary instability in annular channel flow with the axial temperature gradient has been employed in the work [8]. The same direction of the gas motion and thermocapillary motion produces a destabilizing effect on the system, whereas the opposite directions of the gas and thermocapillary motion can be stabilizing or destabilizing subject to the gas flow rate.

The instability analysis conducted by Benselama et al. [9,10] involves the instabilities arising in the streamwise direction, whereas it makes sense to take into account the instabilities arising in both directions, i.e. streamwise and orthogonal to the wall. Another drawback of the studies performed in these works is the use of the perturbation technique rather than the analytical solution to model the main flow and heat transfer.

A series of works is devoted to direct numerical modeling of thermocapillary instability. For instance, Benard–Marangoni instability was studied in the work [11] using the Volume of Fluid (VOF) method. This approach employed to model (a) thermocapillary migration of a droplet in a fluid, (b) thermocapillary convection in a liquid layer, and (c) Marangoni convection due to Benard–Marangoni instability demonstrated a fair agreement with experiments. The methodology of VOF was employed in the work [12] for numerical simulations of Marangoni convection of binary fluids in a closed microcavity. For simple fluids, surface tension reduces at higher temperatures, which causes thermal Marangoni convection forcing the liquid to move out from hot regions that leads to film dryout. In binary fluids, the Marangoni convection arose due to concentration gradients. In self-rewetting fluids, surface tension increases at higher temperatures above a critical value, therefore Marangoni convection pushes liquid towards hot regions, which helps avoiding the film dryout. Direct modeling of the short- and long-wave modes of Marangoni instability was performed in the work [13]. It was demonstrated that convection cells result in short-wave instability, whereas long-wave instability leads to the film rupture. Authors of the investigation [14] focused on the direct modeling of hydrodynamic stability of thermocapillary flow in a

finite-size liquid bridge heated from above and placed in a passive gas environment. Here critical Reynolds numbers and the wave number were determined as the function of the Biot number. Different aspects of the thermocapillary instability have been studied using the direct numerical modeling approach also in the works [15–17].

Thermocapillary instability has been studied also experimentally, whereas the most interesting results from our point of view are presented in the works [18–21].

Different effects of the thermocapillary instability on the parameters of the main fluid flow and heat transfer were studied in the works [19,22–24].

In the light of the literature review made above the objectives of the present work were:

(1) To develop a novel 2D model for the thermocapillary instability of a thin liquid film including an analytical solution for the unperturbed velocity components and the evaporating thin film in the transition region under the boundary conditions of (a) mechanical interaction between the liquid and vapor phases and (b) stationary vapor above the interface.
(2) To develop a novel model for the problem of the thermocapillary instability in a thin film based on the linear perturbation method with account for the surface and London–van der Waals forces. The instability analysis will be performed using the respectively modified Orr–Sommerfeld equation. The resulting solution will be analyzed in order to elucidate effects on the critical Reynolds number of the different influencing physical parameters, such as the capillary and Marangoni numbers.

2. Governing equations

The 2D unsteady fluid flow and heat transfer of an incompressible fluid is described by the following governing equations:

$$\rho\left(\frac{\partial u}{\partial t}+u\frac{\partial u}{\partial x}+\upsilon\frac{\partial u}{\partial y}\right)=-\frac{\partial p}{\partial x}+\mu\left(\frac{\partial^2 u}{\partial x^2}+\frac{\partial^2 u}{\partial y^2}\right), \tag{1}$$

$$\rho\left(\frac{\partial \upsilon}{\partial t}+u\frac{\partial \upsilon}{\partial x}+\upsilon\frac{\partial \upsilon}{\partial y}\right)=-\frac{\partial p}{\partial y}+\mu\left(\frac{\partial^2 \upsilon}{\partial x^2}+\frac{\partial^2 \upsilon}{\partial y^2}\right), \tag{2}$$

$$\frac{\partial u}{\partial x}+\frac{\partial \upsilon}{\partial y}=0, \tag{3}$$

$$c\rho\left(\frac{\partial T}{\partial t}+u\frac{\partial T}{\partial x}+\upsilon\frac{\partial T}{\partial y}\right)=k\left(\frac{\partial^2 T}{\partial x^2}+\frac{\partial^2 T}{\partial y^2}\right). \tag{4}$$

We are going to consider the region where the flow can be presented as a thin film (Fig. 1). In frames of the thin film approach Eqs. (1)–(3) for the steady flow can be reduced to following form

$$\mu\frac{d^2u}{dy^2}=\frac{dp}{dx},\qquad \frac{d^2T}{dy^2}=0. \tag{5}$$

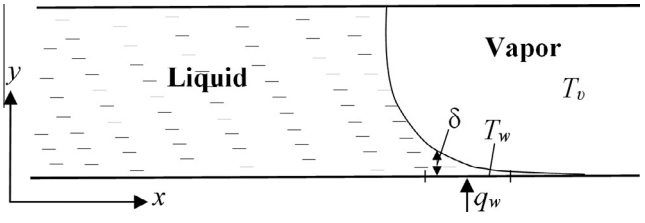

Fig. 1. Schematic of the thermocapillary flow and heat transfer.

Here

$$p=p_{cap}-p_{disj}, \tag{6}$$

where p_{cap} is the capillary pressure, and p_{disj} is the disjoining pressure.

The capillary pressure is determined by the Young–Laplace equation, which can be expressed as follows [9]

$$p_{cap}=\frac{d^2\delta}{dx^2}\frac{\sigma(T)}{\left(1+\left(\frac{d\delta}{dx}\right)^2\right)^{3/2}}=K\sigma(T), \tag{7}$$

where K is curvature, the expression

$$\sigma(T)=\sigma_0-\gamma(T-T_w), \tag{8}$$

determines the interface surface tension. Here σ_0 is the reference surface tension at this reference point, and the parameter $\gamma>0$ (the surface tension gradient with respect to temperature)

$$\gamma=-\left.\frac{\partial\sigma}{\partial T}\right|_{T_w}. \tag{9}$$

is assumed to be constant.

Eq. (8) demonstrates that surface tension decreases with the increasing temperature finally tending to zero as the temperature approaches its critical value [25]

The disjoining pressure

$$p_{disj}=-\frac{A}{\delta^3}, \tag{10}$$

expresses the London–van der Waals molecular interactions [9], whereas A is the dispersion constant associated with the vapor–liquid-solid substrate system.

In this work we consider either of two types of the boundary conditions. The first of them reflects the mechanical interaction between two phases:

$$u=0,\quad T=T_w\quad \text{at}\quad y=0, \tag{11}$$

$$\frac{\partial u}{\partial y}=\frac{\tau}{\mu}\quad kn\frac{\partial T}{\partial y}=\Delta h\dot{m}\quad \text{at}\quad y=\delta, \tag{12}$$

and second states that the vapor is stationary:

$$u=0\quad kn\frac{\partial T}{\partial y}=\Delta h\dot{m}\quad \text{at}\quad y=\delta, \tag{13}$$

In Eqs. (11)–(13), the normal to the interface is defined as

$$n=\frac{1}{\left(1+(d\delta/dx)^2\right)^{1/2}}. \tag{14}$$

The boundary condition (12) was formulated by Nusselt [26], and since then it has been widely used in studies of film condensation of stationary or moving vapor. For stationary vapor the boundary stress friction is zero $\tau=0$, for moving vapor τ can be determined from the friction coefficient, e.g. from the data of [27], like it was done by Nusselt [26]. Both these variants of the boundary conditions were used in the works [28,29] for modeling of condensation and boiling of a nanofluid over a flat surface. The boundary conditions $\tau=0$ and $\tau\neq 0$ will be also employed in this paper, and the unperturbed velocity profile to be obtained on the basis of the condition (12) will take into account both of them. Condition (13) was also used by Ellion [30] in the study of film boiling.

DOI : 10.1016/j.ijheatmasstransfer.2015.07.063

3. Steady solution for the case of mechanical interaction between two phases

This case corresponds to the boundary conditions (11), (12). The integration of system (5) with account for Eqs. (7) and (8) and under the boundary conditions (11), (12) gives

$$u=\frac{\tau y}{\mu}+\left(-\frac{d\delta}{dx}\right)\frac{9Ay(2\delta-y)}{6\mu\delta^4}+\frac{3y(2\delta-y)\sigma_0+\dot{m}\gamma\Delta h y(3\delta^2-y^2)k^{-1}\sqrt{1+(d\delta/dx)^2}}{6\mu(1+(d\delta/dx)^2)^{5/2}}\left(3\left(-\frac{d\delta}{dx}\right)\left(\frac{d^2\delta}{dx^2}\right)^2+\left(1+\left(\frac{d\delta}{dx}\right)^2\right)\frac{d^3\delta}{dx^3}\right),\tag{15}$$

$$\Theta=\frac{\dot{m}\Delta h y\sqrt{1+(d\delta/dx)^2}}{k\Delta T},\tag{16}$$

where

$$\Theta=\frac{T_w-T}{\Delta T},\quad \Delta T=T_w-T_\upsilon.\tag{17}$$

The generalized unperturbed velocity profile (15) obtained with allowance for the condition (12) incorporates both conditions $\tau=0$ and $\tau\neq 0$.

The dimensionless velocity profile looks as

$$U=W\eta+\left(3+(\mathrm{Ca}^*)^{-1}\right)\left(\eta-\frac{\eta^2}{2}\right)+\frac{\mathrm{Ma}^*}{2}\left(\eta-\frac{\eta^3}{3}\right),\tag{18}$$

where

$$\eta=\frac{y}{\delta},\tag{19}$$

$$U=\frac{u\mu\delta^2}{A\left(-\frac{d\delta}{dx}\right)},\tag{20}$$

$$W=\frac{\tau\delta^3}{A\left(-\frac{d\delta}{dx}\right)},\tag{21}$$

$$(\mathrm{Ca}^*)^{-1}=\frac{\sigma_0\mu\delta^2}{\mu A}\frac{\delta^2}{\left(1+\left(\frac{d\delta}{dx}\right)^2\right)^{5/2}\left(-\frac{d\delta}{dx}\right)}\left(3\left(-\frac{d\delta}{dx}\right)\left(\frac{d^2\delta}{dx^2}\right)^2+\left(1+\left(\frac{d\delta}{dx}\right)^2\right)\frac{d^3\delta}{dx^3}\right),\tag{22}$$

$$\mathrm{Ma}^*=\frac{\Delta T\gamma\delta^3 a\Delta h}{kA}\frac{\delta^2}{\left(1+\left(\frac{d\delta}{dx}\right)^2\right)^2\left(-\frac{d\delta}{dx}\right)}\left(3\left(-\frac{d\delta}{dx}\right)\left(\frac{d^2\delta}{dx^2}\right)^2+\left(1+\left(\frac{d\delta}{dx}\right)^2\right)\frac{d^3\delta}{dx^3}\right).\tag{23}$$

The dimensionless velocity (21), which serves as the scaling velocity, arises in a natural way while non-dimensionalising the expression (15) for the velocity profile.

Thus the mathematical model of the main fluid flow involves two important similarity criteria: the capillary number Ca^*, Eq. (22), and the modified Marangoni number Ma^*, Eq. (24). The capillary number represents the relation between effect of viscous forces and surface tension, which acts across the interface between the liquid and the gas or between two immiscible liquids. The Marangoni number represents the relation between thermally dependent surface tension forces and viscous forces. Hence Marangoni number also takes into account the dependence of the surface tension on the temperature. We will use further several definitions of the Marangoni number, such as Ma, Ma^* and Ma^{**} (see Nomenclature), arising from the different mathematical forms of the solutions derived below.

Here we used following equation for the mass flux of the vapor [15]

$$\dot{m}=a\Delta T,\tag{24}$$

where a is constant.

Eq. (24) can be justified by the following physical reasoning and mathematical derivations. If we accept that in the heating region $T_w=const$ and $T_\upsilon=const$, than in accordance with Benselama et al. [9]

$$\dot{m}=a(T_w-T_\upsilon)+b(p_l-p_\upsilon).\tag{25}$$

Here [10]

$$a=\frac{2\alpha_m}{2-\alpha_m}\left(\frac{M}{2\pi RT_\upsilon}\right)^{1/2}\left(\frac{p_\upsilon M\Delta h}{RT_\upsilon^2}\right),\quad b=\frac{2\alpha_m}{2-\alpha_m}\left(\frac{M}{2\pi RT_\upsilon}\right)^{1/2}\left(\frac{V_l p_\upsilon}{RT_\upsilon}\right),\tag{26}$$

where R is the universal gas constant, M is the molar mass, V_l is the molar volume of the liquid.

With respect to the second term, it can be shown that $p_l-p_\upsilon\sim\frac{\sigma}{R}$. The curvature varies weakly over the length of the contact line, therefore the value p_l-p_υ is constant. Besides, the phase transition occurs at the constant pressure, i.e. $p_l\approx p_\upsilon$. Therefore, the second term in Eq. (25) is vanishingly small, which reduces Eq. (25) to Eq. (24). Neglecting the second term in Eq. (25) is not crucially important in the instability model. The mass flux of the vapor $\dot{m}$ can be incorporated in the dimensionless parameters with account for the second term in Eq. (25). It will not affect the profile of the unperturbed velocity and, accordingly, the criteria of instability.

The form of the Marangoni number Ma^* in Eq. (23) is different from its traditional definition. The dimensionless complex denoted here as the Marangoni number was obtained in a natural way in course of non-dimensionalising of the relation for the velocity profile (15). This complex was denoted as the Marangoni number, because it is close to the classical definition of this parameter. Denoting this complex in a different way would have introduced a new dimensionless parameter, which we tried to avoid. A relation between the modified Marangoni number Ma^* and its classical definition presented in [9] gives the following relation

$$\mathrm{Ma}^*=\underbrace{\frac{\Delta T\gamma\delta c\rho}{\mu k}}_{\mathrm{Ma}}\underbrace{\frac{k\mu\delta^2}{c\rho\delta A}}_{\mathrm{Pe}^{-1}}\underbrace{\frac{a\Delta h\,\delta}{k}}_{\kappa}\frac{\delta^2}{\left(1+\left(\frac{d\delta}{dx}\right)^2\right)^2\left(-\frac{d\delta}{dx}\right)}\left(3\left(-\frac{d\delta}{dx}\right)\left(\frac{d^2\delta}{dx^2}\right)^2+\left(1+\left(\frac{d\delta}{dx}\right)^2\right)\frac{d^3\delta}{dx^3}\right),\tag{27}$$

where

$$\mathrm{Ma}=\frac{\Delta T\gamma\delta c\rho}{\mu k},\tag{28}$$

$$\mathrm{Pe}=\frac{c\rho\delta A}{k\mu\delta^2},\tag{29}$$

$$\kappa=\frac{a\Delta h\,\delta}{k}.\tag{30}$$

Parameter κ was introduced by [10]. As one can see from Eq. (27), all these three parameters can be replaced by one cumulative parameter that is more convenient while analyzing the results.

To model the instability, it is sometimes convenient to introduce the new variable

$$\xi = 2\eta - 1. \tag{31}$$

Using this variable, the profile (15) can be rewritten as

$$U = \frac{1}{2}W(\xi+1) + \frac{1}{8}\left(3 + (\mathrm{Ca}^*)^{-1}\right)(3-\xi)(\xi+1) + \frac{1}{48}\mathrm{Ma}^*(\xi+1)(11-\xi^2-2\xi). \tag{32}$$

The modified capillary Ca^* and Marangoni Ma^* numbers include derivatives of the different orders from the film thickness respect to the longitudinal variable x. This is not convenient for the instability analysis. Then let us try to exclude these derivatives, with the functions of the coordinate x themselves still remaining in Eqs. (22) and (27). For this purpose, one can use the mass balance equation [9,29]

$$-\frac{dG}{dx} = \dot{m}, \tag{33}$$

where flow rate per unit length is

$$G = \rho\int_0^{\delta(x)} u dy. \tag{34}$$

Substitution of Eq. (15) into Eq. (34) gives

$$G = \frac{\rho}{\mu}\left(\frac{\tau\delta^2}{2} + \left(-\frac{d\delta}{dx}\right)\frac{A}{\delta} + \frac{\delta^3\left(8k\sigma_0 + 5\dot{m}\gamma\Delta h\,\delta\sqrt{1+(d\delta/dx)^2}\right)}{24k\left(1+(d\delta/dx)^2\right)^{5/2}}\left(3\left(-\frac{d\delta}{dx}\right)\left(\frac{d^2\delta}{dx^2}\right)^2 + \left(1+\left(\frac{d\delta}{dx}\right)^2\right)\frac{d^3\delta}{dx^3}\right)\right). \tag{35}$$

An attempt to integrate Eq. (33) with account for Eq. (35) did not succeed in deriving an exact analytical solution. However, to obtain the instability criteria in frames of our approach, we do not need a strictly justifiable exact solution for the film thickness, because it in no way affects the shape of the unperturbed velocity profile (32). That is why let us make a simplifying assumption that the film thickness is only weakly dependent on the shear stress friction τ at the boundary between the liquid and vapor phases, as well as on the curvature effects. Given this assumption, one can neglect the first and the third terms in the velocity profile (35). The result is

$$G = \left(-\frac{d\delta}{dx}\right)\frac{A\rho}{\mu\delta}. \tag{36}$$

Taking into account Eq. (36), one solve Eq. (34) in the following form

$$\delta = \delta_0\exp\left(-\frac{\dot{m}\mu x^2}{2A\rho}\right), \tag{37}$$

where the initial film thickness δ_0 can be set equal to the diameter of the capillary.

Using Eq. (37) and eliminating x, one can obtain the following expressions

$$-\frac{d\delta}{dx} = \sqrt{MS}, \tag{38}$$

$$3\delta^2\left(-\frac{d\delta}{dx}\right)\left(\frac{d^2\delta}{dx^2}\right)^2 = (1-S)^2\sqrt{9M^5S}, \tag{39}$$

$$\delta^2\left(1+\left(\frac{d\delta}{dx}\right)^2\right)\frac{d^3\delta}{dx^3} = (1+MS)(3-S)\sqrt{M^3S}, \tag{40}$$

where

$$M = \frac{\dot{m}\mu\delta^2}{\rho A} \quad S = 2\ln\left(\frac{\delta_0}{\delta}\right). \tag{41}$$

Taking into account Eqs. (38)–(40), one can rewrite Eqs. (23) and (28) as

$$(\mathrm{Ca}^*)^{-1} = \frac{\sigma_0\delta^2}{A}\frac{(1-S)^2\sqrt{9M^5S} + (1+MS)(3-S)\sqrt{M^3S}}{(1+MS)^{5/2}\sqrt{MS}}, \tag{42}$$

$$\mathrm{Ma}^* = \underbrace{\frac{\Delta T\gamma\delta c\rho}{\mu k}}_{\mathrm{Ma}}\underbrace{\frac{k\mu\delta^2}{c\rho\delta A}}_{\mathrm{Pe}^{-1}}\underbrace{\frac{a\Delta h\,\delta}{k}}_{\kappa}\frac{(1-S)^2\sqrt{9M^5S} + (1+MS)(3-S)\sqrt{M^3S}}{(1+MS)^2\sqrt{MS}}. \tag{43}$$

Using the notations of the authors of the work [9], one can demonstrate that $M = \frac{\dot{m}\mu\delta^2}{\rho A} \sim \frac{\dot{m}}{\rho u^*}\frac{\delta}{l^*}$, where u^* and l^* are the characteristic scales of the longitudinal velocity and the length. At low values of overheating, the evaporative mass flux crossing the interface $\dot{m}$ is smaller than the term ρu^*, whereas $\delta/l^* \ll 1$. Therefore, we one can assume that $M < 1$. Expanding further Eqs. (42) and (43) in the series with respect to parameter M brings

$$(\mathrm{Ca}^*)^{-1} \approx \frac{\sigma_0\delta^2}{A}(3-S)M = \mathrm{Ca}^{-1}, \tag{44}$$

$$\mathrm{Ma}^* \approx \underbrace{\frac{\Delta T\gamma\delta c\rho}{\mu k}}_{\mathrm{Ma}}\underbrace{\frac{k\mu\delta^2}{c\rho\delta A}}_{\mathrm{Pe}^{-1}}\underbrace{\frac{a\Delta h\,\delta}{k}}_{\kappa}(3-S)M = \mathrm{Ma}^{**}, \tag{45}$$

which are valid under the condition

$$S < 3 \Rightarrow \frac{\delta_0}{\delta} < 4.8. \tag{46}$$

Using the continuity equation (3) and taking into account the boundary condition $V = 0$ at $y = 0$, one can derive an equation for the transverse velocity component in the general form not involving the aforementioned simplified model, Eq. (37), for the film thickness

$$V = \frac{\upsilon\mu\delta^2}{A\left(-\frac{d\delta}{dx}\right)} = \frac{\eta^2}{2}\left(9-4\eta\right)\left(-\frac{d\delta}{dx}\right) + (3-\eta)\delta\frac{d^2\delta}{dx^2}\left(-\frac{d\delta}{dx}\right)^{-1} - \frac{\sigma_0\delta^2\eta^2}{2A\left(1+\left(\frac{d\delta}{dx}\right)^2\right)^{7/2}\left(-\frac{d\delta}{dx}\right)}\left(\delta^2\left(\frac{d^2\delta}{dx^2}\right)^2(3-\eta)\left(4\left(\frac{d\delta}{dx}\right)^2-1\right)\right.$$
$$\left.\delta\frac{d^2\delta}{dx^2}-3\left(\left(\frac{d\delta}{dx}\right)^2+\left(\frac{d\delta}{dx}\right)^4\right)\right) + \left(\frac{d\delta}{dx}\right)+\left(\frac{d\delta}{dx}\right)^3\left(1+\left(\frac{d\delta}{dx}\right)^2-3(3-\eta)\delta\frac{d^2\delta}{dx^2}\right)\delta^2\frac{d^3\delta}{dx^3}+\frac{1}{3}(3-\eta)\left(1+\left(\frac{d\delta}{dx}\right)^2\right)^2\delta^3\frac{d^4\delta}{dx^4}\Bigg)$$
$$-\underbrace{\frac{\Delta T\gamma\delta c\rho}{\mu k}}_{\mathrm{Ma}}\underbrace{\frac{k\mu\delta^2}{c\rho\delta A}}_{\mathrm{Pe}^{-1}}\underbrace{\frac{a\Delta h\,\delta}{k}}_{\kappa}\frac{\eta^2}{24\left(1+\left(\frac{d\delta}{dx}\right)^2\right)^3\left(-\frac{d\delta}{dx}\right)}\left(12\frac{d\delta}{dx}\left(1+\left(\frac{d\delta}{dx}\right)^2\right)\delta^2\left(3\left(-\frac{d\delta}{dx}\right)\left(\frac{d^2\delta}{dx^2}\right)^2+\left(1+\left(\frac{d\delta}{dx}\right)^2\right)\frac{d^3\delta}{dx^3}\right)\right.$$
$$+(\eta^2-6)\delta^3\left(3-9\left(\frac{d\delta}{dx}\right)^2\right)\left(\frac{d^2\delta}{dx^2}\right)^3$$
$$\left.+8\frac{d\delta}{dx}\left(1+\left(\frac{d\delta}{dx}\right)^2\right)\frac{d^2\delta}{dx^2}\frac{d^3\delta}{dx^3}-\left(1+\left(\frac{d\delta}{dx}\right)^2\right)^2\frac{d^4\delta}{dx^4}\right)\Bigg) \tag{47}$$

Assuming that $M < 1$, one can reduce Eq. (47) to

$$V=\frac{\eta^2(\eta-3+(12-5\eta)S)\sqrt{M}}{2\sqrt{S}} \tag{48}$$

or

$$V=\frac{(1+\xi)^2(\xi-5+(19-5\xi)S)\sqrt{M}}{16\sqrt{S}}. \tag{49}$$

4. Steady solution for the stationary vapor

This case corresponds to the boundary conditions (11), (13). The velocity profile can be written as

$$u=\left(-\frac{d\delta}{dx}\right)\frac{9Ay(\delta-y)}{6\mu\delta^4}+\frac{3y(\delta-y)\sigma_0+\dot{m}\gamma\Delta h y(\delta^2-y^2)k^{-1}\sqrt{1+(d\delta/dx)^2}}{6\mu(1+(d\delta/dx)^2)^{5/2}}$$
$$\left(3\left(-\frac{d\delta}{dx}\right)\frac{d^2\delta}{dx^2}\right)^2+\left(1+\left(\frac{d\delta}{dx}\right)^2\right)\frac{d^3\delta}{dx^3}\Bigg). \tag{50}$$

The dimensionless velocity profile takes the following form

$$U=\left(\frac{3}{2}+\frac{(\mathrm{Ca}^*)^{-1}}{2}\right)(\eta-\eta^2)+\frac{\mathrm{Ma}^*}{6}\eta(1-\eta^2) \tag{51}$$

or

$$U=\left(\frac{3}{8}+\frac{(\mathrm{Ca}^*)^{-1}}{8}\right)(1-\xi^2)+\frac{\mathrm{Ma}^*}{48}(\xi+3)(1-\xi^2), \tag{52}$$

$$U''=-\left(\frac{3}{4}+\frac{(\mathrm{Ca}^*)^{-1}}{4}\right)-\frac{\mathrm{Ma}^*}{8}(1+\xi). \tag{53}$$

Based on the aforementioned simplified assumption regarding the film thickness and thus neglecting the second term in the velocity profile (50) responsible for the curvature effects, one can repeat the derivations from the previous section and finally come to the following equations

$$\delta=\delta_0\exp\left(-\frac{2\dot{m}\mu x^2}{A\rho}\right), \tag{54}$$

$$-\frac{d\delta}{dx}=2\sqrt{MS}, \tag{55}$$

$$3\delta^2\left(-\frac{d\delta}{dx}\right)\left(\frac{d^2\delta}{dx^2}\right)^2=96(1-S)^2\sqrt{M^5S}, \tag{56}$$

$$\delta^2\left(1+\left(\frac{d\delta}{dx}\right)^2\right)\frac{d^3\delta}{dx^3}=(1+4MS)(3-S)8\sqrt{M^3S}. \tag{57}$$

For this case, Eqs. (44) and (45) are substituted with

$$(\mathrm{Ca}^*)^{-1}\approx 4\mathrm{Ca}^{-1}, \tag{58}$$

$$\mathrm{Ma}^*\approx 4\mathrm{Ma}^{**}, \tag{59}$$

Then the dimensionless velocity profile is

$$U=\left(\frac{3}{2}+2\mathrm{Ca}^{-1}\right)(\eta-\eta^2)+\frac{2}{3}\mathrm{Ma}^{**}\eta(1-\eta^2) \tag{60}$$

or

$$U=\left(\frac{3}{8}+\frac{\mathrm{Ca}^{-1}}{2}\right)(1-\xi^2)+\frac{\mathrm{Ma}^{**}}{12}(\xi+3)(1-\xi^2), \tag{61}$$

$$U''=-\left(\frac{3}{4}+\mathrm{Ca}^{-1}\right)-\frac{\mathrm{Ma}^{**}}{2}(1+\xi). \tag{62}$$

The transverse velocity component is

$$V=\frac{\upsilon\mu\delta^2}{A(-\frac{d\delta}{dx})}=\frac{\eta^2(3-2\eta)}{4}\left(4\frac{d\delta}{dx}+\delta\frac{d^2\delta}{dx^2}\left(-\frac{d\delta}{dx}\right)^{-1}\right)$$
$$+\frac{\sigma_0\delta^2\eta^2(2\eta-3)\delta^3}{12A\left(1+\left(\frac{d\delta}{dx}\right)^2\right)^{7/2}\left(-\frac{d\delta}{dx}\right)}\left(3\left(4\left(\frac{d\delta}{dx}\right)^2-1\right)\left(\frac{d^2\delta}{dx^2}\right)^3\right.$$
$$\left.-9\left(\frac{d\delta}{dx}\right)+\left(\frac{d\delta}{dx}\right)^3\right)\frac{d^2\delta}{dx^2}\frac{d^3\delta}{dx^3}+\left(1+\left(\frac{d\delta}{dx}\right)^2\right)^2\frac{d^4\delta}{dx^4}\Bigg)$$
$$+\underbrace{\frac{\Delta T\gamma\delta c\rho}{\mu k}}_{\mathrm{Ma}}\underbrace{\frac{k\mu\delta^2}{c\rho\delta A}}_{\mathrm{Pe}^{-1}}\underbrace{\frac{a\Delta h\,\delta}{k}}_{\kappa}\frac{\eta^2(\eta^2-2)\delta^3}{24\left(1+\left(\frac{d\delta}{dx}\right)^2\right)^3\left(-\frac{d\delta}{dx}\right)}$$
$$\times\left(\left(9\left(\frac{d\delta}{dx}\right)^2-3\right)\left(\frac{d^2\delta}{dx^2}\right)^3+8\left(-\frac{d\delta}{dx}\right)\left(1+\left(\frac{d\delta}{dx}\right)^2\right)\frac{d^2\delta}{dx^2}\frac{d^3\delta}{dx^3}\right.$$
$$\left.+\left(1+\left(\frac{d\delta}{dx}\right)^2\right)^2\frac{d^4\delta}{dx^4}\right). \tag{63}$$

Setting $M<1$, one can simplify Eq. (47) as

$$V=\frac{2\eta^2(2\eta-3)(1+3S)\sqrt{M}}{\sqrt{S}} \tag{64}$$

or

$$V=\frac{(1+\xi)^2(\xi-2)(1+3S)\sqrt{M}}{2\sqrt{S}}. \tag{65}$$

5. Perturbation equations and Squire's theorem

For the 2D instability analysis, we use the method of the linear perturbation. Let us present the velocity and pressure as

$$u(t,x,y)=u_0(y)+u'(t,x,y), \tag{66}$$

$$\upsilon(t,x,y)=\upsilon_0(y)+\upsilon'(t,x,y), \tag{67}$$

$$p(t,x,y)=p_0(x,y)+p'(t,x,y), \tag{68}$$

where u_0, υ_0 and p_0 are the unperturbed (basic flow) parameters. As one can see above, the unperturbed velocities (15), (47), (50) and (63) are in general the functions of longitudinal coordinates x. However, as shown in [31], in frames of the boundary layer approach the stability analysis can be performed under assumption that the basic (i.e. unperturbed) velocities are the functions of the only transverse coordinate y. We will therefore also assume that the basic velocity is the function of the transverse coordinate depending also on the capillary and Marangoni numbers. The velocity components u', υ' and the pressure p' are the perturbed values.

The substitution of Eqs. (66)–(68) in the Eqs. (1)–(3) and further linearization yields

$$\rho\left(\frac{\partial u'}{\partial t}+u_0\frac{\partial u'}{\partial x}+\upsilon'\frac{\partial u_0}{\partial y}+\upsilon_0\frac{\partial u'}{\partial y}\right)=-\frac{\partial p'}{\partial x}+\mu\left(\frac{\partial^2 u'}{\partial x^2}+\frac{\partial^2 u'}{\partial y^2}\right), \tag{69}$$

$$\rho\left(\frac{\partial \upsilon'}{\partial t}+u_0\frac{\partial \upsilon'}{\partial x}+\upsilon'\frac{\partial \upsilon_0}{\partial y}+\upsilon_0\frac{\partial \upsilon'}{\partial y}\right)=-\frac{\partial p'}{\partial y}+\mu\left(\frac{\partial^2 \upsilon'}{\partial x^2}+\frac{\partial^2 \upsilon'}{\partial y^2}\right), \tag{70}$$

$$\frac{\partial u'}{\partial y}+\frac{\partial \upsilon'}{\partial y}=0. \tag{71}$$

Let us rewrite the perturbed velocity through the stream function as

$$u' = \frac{\partial \psi}{\partial y}, \quad \upsilon' = -\frac{\partial \psi}{\partial x}, \quad \psi = \tilde{\varphi}(y)\exp(i(\tilde{\alpha}x - \tilde{\beta}t)). \tag{72}$$

Pressure can be eliminated from Eqs. (69) and (70) using the classical approach: Eq. (69) is differentiated with respect to y, and Eq. (70) is differentiated with respect to x. The resulting equations are subtracted one from the other. Thus, substituting Eq. (72) into Eqs. (69)–(71) and eliminating the pressure results in the following equation

$$(U-c)(\varphi'' - \alpha^2\varphi) - U''\varphi = -\frac{i}{\alpha \mathrm{Re}}(\varphi'''' - 2\alpha^2\varphi'' + \alpha^4\varphi) \underbrace{-\frac{iV}{\alpha}(\alpha^2\varphi' - \varphi''') - \frac{iV'}{\alpha}(\alpha^2\varphi - \varphi'')}_{\mathrm{I}}, \tag{73}$$

In this equation, in analogy to the studies of the instability in frames of the boundary layer approach [31,32], the unperturbed velocity profiles are the functions of the dimensionless variable $\xi = 2\eta - 1 = 2y/\delta - 1$, which obviously incorporates the film thickness.

Basic velocities U is defined by Eqs. (33) or (61), and V is defined by Eqs. (48) or (65) depending on the form of the boundary conditions. Eq. (73) is the modified Orr–Sommerfeld equation, which includes the effect of the transverse basic velocity. Here the terms denoted as "I" are the modification as compared to the classical Orr–Sommerfeld equation; the primes denote the derivatives with respect to ξ;

$$\alpha = \tilde{\alpha}(\delta/2), \quad c = \tilde{\beta}/\tilde{\alpha} = c_r + ic_i, \quad \varphi = \tilde{\varphi}\Big/\left(\frac{A}{\mu\delta^2}\left(-\frac{d\delta}{dx}\right)\frac{\delta}{2}\right) = \tilde{\varphi}\Big/\left(\frac{A}{2\mu\delta}\left(-\frac{d\delta}{dx}\right)\right), \quad \mathrm{Re} = \frac{A\rho}{2\mu^2\delta}\left(-\frac{d\delta}{dx}\right), \tag{74}$$

where c_r is the velocity of the propagation of the disturbance wave; and c_i is the parameter that determines the rate of the damping (or amplification) of the disturbances.

For the 3D instability analysis, let us introduce the following values

$$u(t,x,y,z) = u_0(y) + u'(t,x,y,z), \tag{75}$$

$$\upsilon(t,x,y,z) = \upsilon_0(y) + \upsilon'(t,x,y,z), \tag{76}$$

$$w(t,x,y,z) = w'(t,x,y,z), \tag{77}$$

$$p(t,x,y,z) = p_0(x,y) + p'(t,x,y,z). \tag{78}$$

In this case, the perturbation equations are

$$\rho\left(\frac{\partial u'}{\partial t} + u_0\frac{\partial u'}{\partial x} + \upsilon'\frac{\partial u_0}{\partial y} + \upsilon_0\frac{\partial u'}{\partial y}\right) = -\frac{\partial p'}{\partial x} + \mu\left(\frac{\partial^2 u'}{\partial x^2} + \frac{\partial^2 u'}{\partial y^2} + \frac{\partial^2 u'}{\partial z^2}\right), \tag{79}$$

$$\rho\left(\frac{\partial \upsilon'}{\partial t} + u_0\frac{\partial \upsilon'}{\partial x} + \upsilon'\frac{\partial \upsilon_0}{\partial y} + \upsilon_0\frac{\partial \upsilon'}{\partial y}\right) = -\frac{\partial p'}{\partial y} + \mu\left(\frac{\partial^2 \upsilon'}{\partial x^2} + \frac{\partial^2 \upsilon'}{\partial y^2} + \frac{\partial^2 \upsilon'}{\partial z^2}\right), \tag{80}$$

$$\rho\left(\frac{\partial w'}{\partial t} + u_0\frac{\partial w'}{\partial x} + \upsilon_0\frac{\partial w'}{\partial y}\right) = -\frac{\partial p'}{\partial z} + \mu\left(\frac{\partial^2 w'}{\partial x^2} + \frac{\partial^2 w'}{\partial y^2} + \frac{\partial^2 w'}{\partial z^2}\right), \tag{81}$$

$$\frac{\partial u'}{\partial y} + \frac{\partial \upsilon'}{\partial y} + \frac{\partial w'}{\partial z} = 0. \tag{82}$$

The perturbation values are

$$u' = \tilde{u}_A(y)\exp\left(i(\tilde{\alpha}x + \tilde{\gamma}z - \tilde{\beta}t)\right), \tag{83}$$

$$\upsilon' = \tilde{\upsilon}_A(y)\exp\left(i(\tilde{\alpha}x + \tilde{\gamma}z - \tilde{\beta}t)\right), \tag{84}$$

$$w' = \tilde{w}_A(y)\exp\left(i(\tilde{\alpha}x + \tilde{\gamma}z - \tilde{\beta}t)\right), \tag{85}$$

$$p' = \tilde{p}_A(y)\exp\left(i(\tilde{\alpha}x + \tilde{\gamma}z - \tilde{\beta}t)\right), \tag{86}$$

Substituting Eqs. (83)–(86) into Eqs. (79)–(82) and excluding the parameters $\tilde{u}_A$, $\tilde{w}_A$ and $\tilde{p}_A$, one can come to the equation

$$(U-c)(\upsilon_A'' - \chi^2\upsilon_A) - U''\upsilon_A = -\frac{i}{\alpha \mathrm{Re}}(\upsilon_A'''' - 2\chi^2\upsilon'' + \chi^4\upsilon_A) \underbrace{-\frac{iV}{\alpha}(\chi^2\upsilon_A' - \upsilon_A''') - \frac{iV'}{\alpha}(\chi^2\upsilon_A - \upsilon_A'')}_{\mathrm{I}}, \tag{87}$$

where

$$\chi = (\delta/2)\sqrt{\tilde{\alpha}^2 + \tilde{\gamma}^2}, \quad \upsilon_A = \tilde{\upsilon}_A\Big/\left(\frac{A}{\mu\delta^2}\left(-\frac{d\delta}{dx}\right)\right). \tag{88}$$

Given the classical Orr–Sommerfeld equation, one can apply the well-known Squire's theorem [33]. According to this theorem, for the 2D flow the 2D disturbances are more dangerous than the three-dimensional disturbances. In turn, this means that that the critical Reynolds number can be computed by considering the 2D disturbances only. It can be demonstrated that Squire's theorem remains in force as applied to the present situation. Eq. (86) can be transformed using the Squire's transformation

$$\alpha^* = \chi = (\delta/2)\sqrt{\tilde{\alpha}^2 + \tilde{\gamma}^2}, \quad \varphi^* = \upsilon_A, \quad \frac{V^*}{\alpha^*} = \frac{V}{\alpha}, \quad \alpha^*\mathrm{Re}^* = \alpha\mathrm{Re}. \tag{89}$$

One can obtain the transformed equation based on Eq. (87)

$$(U-c)(\varphi^{*\prime\prime} - \alpha^{*2}\varphi^*) - U''\varphi^* = -\frac{i}{\alpha^*\mathrm{Re}^*}(\varphi^{*\prime\prime\prime\prime} - 2\alpha^{*2}\varphi^{*\prime\prime} + \alpha^{*4}\varphi^*) \underbrace{-\frac{iV^*}{\alpha^*}(\alpha^{*2}\varphi^{*\prime} - \varphi^{*\prime\prime\prime}) - \frac{iV^{*\prime}}{\alpha^*}(\alpha^{*2}\varphi^* - \varphi^{*\prime\prime})}_{\mathrm{I}}. \tag{90}$$

It is obvious that this equation has the same mathematical form as the original Eq. (73) with $\tilde{\gamma} = w_A = 0$, so that they thus describe the analogous 2D problems. Since $\alpha^* \geqslant \alpha$, it is evident that $\mathrm{Re}^* \leqslant \mathrm{Re}$. Hence, to find the minimum value of the Reynolds number, it is sufficient to consider only two -dimensional disturbances.

6. Numerical method of solving the eigenvalue problem and validation of the numerical solution

Two methods are used for obtaining the numerical solution of the eigenvalue problem for Eq. (63). The first one is the collocation method [34]. The Galerkin approximation for the amplitude of the stream function can be written as

$$\varphi = \sum_{j=1}^{N} b_j f_j(\xi). \tag{91}$$

For the boundary conditions (11), (12), the trial functions are

$$f_j(\xi) = (2 + \xi - 3\xi^2 - \xi^3 + \xi^4)^j, \tag{92}$$

which satisfy the boundary conditions for the perturbed stream function

$$\xi = -1, \quad \varphi = \varphi' = 0,$$
$$\xi = 1, \quad \varphi = \varphi'' = 0. \tag{93}$$

As discussed below (see beginning of Section 6 "Results and discussion"), flow is always stable under the boundary conditions (11), (12), and it does not make sense to estimate the numerical inaccuracy in this case. For the boundary conditions (11), (13), two different sets of the trial functions are employed here with the purpose to estimate the numerical inaccuracy of the used methodology. The first set of the trial functions is

$$f_j(\xi) = (1-\xi^2)^2 \xi^{2(j-1)}, \tag{94}$$

whereas the second set looks as

$$f_j(\xi) = (1-\xi^2)^2 T_{2j}(\xi), \tag{95}$$

where T_{2j} are the Chebyshev polynomials of the first kind. These sets of the trial function satisfy the following boundary conditions for the perturbed stream function

$$\xi = -1, \quad \varphi = \varphi' = 0,$$
$$\xi = 1, \quad \varphi = \varphi' = 0. \tag{96}$$

In the case where the Chebyshev polynomials are employed to construct the function φ, we used the orthogonal collocation method. In frames of this method, the residuals are calculated in the points where the Chebyshev polynomials are equal to zero. This approach leads to the minimization of the maximum inaccuracy [34].

In frames of another approach for the solution of the eigenvalue problem for Eq. (73), we used CHEBFUN computing environment [35]. In comparison with the collocation method, this approach does not require using different trial functions.

Test computations were performed to validate the numerical code as well as the choice of the basis functions for the first method. The validation was conducted for the basic Poiseuille flow [36]

$$U = 1 - \xi^2, \quad V = 0. \tag{97}$$

This test has demonstrated that for $N = 300$ the difference in the critical Reynolds number Re_{cr} resulting from using the different sets of trial functions (specified by Eqs. (94) and (95), respectively) was less than 1%. The results obtained on the basis of the collocation method agree well with the results provided by CHEBFUN computing environment (less than 1%).

7. Results and discussion

The calculations of the instability criteria for the basic velocity profiles (32), (49) revealed that all perturbations are damped for any values of the parameters W, Ca^* and Ma^*, as well as for $M < 1$ and $S < 3$, i.e. in this case the flow is stable. This situation is similar to the pattern that emerges in the study of the classical boundary layer when on the borders of the simulated domain the main flow velocity is not zero. According to the Rayleigh's second theorem of stability [36], the velocity of propagation of the neutral disturbances c_r in the boundary layer is smaller then the maximum velocity. Obviously, in this case, the conditions where this theorem holds are not satisfied, and the critical layer (where $U = c_r$) that serves as the resonator of onset of the perturbations cannot emerge in the film, i.e. the perturbations do not penetrate into the film. From the mathematical point of view, this phenomenon can be explained by the results of the investigations of the instability in the boundary layer in the presence of a longitudinal pressure gradient (as in our case) performed by [32]. These studies showed that in the hydrodynamic instability the curvature of the velocity profile of the base flow (U'')) plays a significant role. This conclusion is in the agreement with the first Rayleigh theorem of stability (the so-called point of inflexion criterion), according to which the velocity profiles which possess a point of inflexion are unstable [36]. The studies of the instability in the gradient boundary layer [32] revealed that the approximation of the unperturbed velocity profiles by the classic four-term Pohlhausen polynomial proved to be insufficient, since this approximation of the velocity profile curvature is quite different from the curvature of the real profile. In this regard, an approximation of the velocity profiles for the basic flow was performed by [32] on the basis of six-term polynomials, which enabled describing the velocity profile curvature with an acceptable accuracy. Obviously, such a situation arises also in our case, where the unperturbed velocity profile in the film subject to the pressure gradient is described by the third-order polynomials.

The situation is different for the undisturbed velocity profile (61), whose form is closer to the classical Poiseuille velocity profile. As calculations showed, the instability indeed set on in this case. For the case of $Ca^{-1} = Ma^{**} = 0$, the calculations yield the instability criterion

$$Re_{cr} = 15393, \tag{98}$$

which corresponds to the critical wavenumber $\alpha_{cr} = 1.02$, i.e. to the point of minimum on the neutral stability curve obtained under the condition of the neutral disturbances $c_i = 0$. The computations have also shown that the inclusion of the unperturbed transverse velocity component (65) has little effect on the value of the critical Reynolds number (less than 1.5%). Additional computations under conditions of $Ca^{-1} > 0$ and $Ma^{**} > 0$ confirmed this trend, so that one can conclude that the transverse velocity component can be ignored in the instability analysis.

The further calculations of the instability were performed for the case of $Ca^{-1} > 0$ and $Ma^{**} = 0$. This case corresponds to the constant value of the surface tension, i.e. the case where the surface tension does not depend on the temperature. In this case the unperturbed velocity profile still has the form of the Poiseuille profile, but the maximum value (amplitude) of the velocity increases with the increasing values of the parameter Ca^{-1}. Because the unperturbed velocity profile shape is insensitive to the increase in the parameter Ca^{-1}, the critical wave number $\alpha_{cr} = 1.02$ remains unchanged. However, due to the increase in the unperturbed velocity amplitude, the flow becomes less stable, and the critical Reynolds number decreases monotonically with the increasing values of the parameter Ca^{-1} (see Fig. 2 and Table 1).

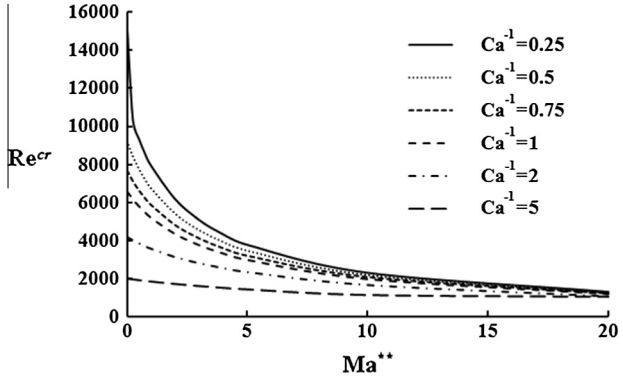

Fig. 2. Critical value of Reynolds number vs Ma^{**} at Ca^{-1} = idem.

Table 1
Critical Reynolds numbers Re_{cr} and critical wave numbers α_{cr} depending on the modified Marangoni number Ma^{**} and inverse capillary number Ca^{-1}.

Ma^{**}	0		0.25		0.5		0.75		1		2		3		4		5		10		20	
Ca^{-1}	Re_{cr}	α_{cr}	Re_{cr}	α_{cr}	Re_{cr}	α_{cr}	Re_{cr}	α_{cr}	Re_{cr}	α_{cr}	Re_{cr}	α_{cr}	Re_{cr}	α_{cr}	Re_{cr}	α_{cr}	Re_{cr}	α_{cr}	Re_{cr}	α_{cr}	Re_{cr}	α_{cr}
0	15393	1.02																				
0.25	11545	1.02	10298	1.014	9344	1.007	8572	1.003	7942	0.998	6181	0.983	5090	0.97	4336	0.959	3780	0.952	2312	0.937	1305	0.92
0.5	9236	1.02	8416	1.016	7759	1.013	7213	1.009	6749	1.005	5418	0.991	4551	0.976	3933	0.966	3469	0.96	2189	0.945	1264	0.925
0.75	7697	1.02	7117	1.017	6636	1.015	6230	1.011	5875	1.009	4827	0.997	4121	0.985	3604	0.975	3206	0.968	2087	0.95	1225	0.929
1	6597	1.02	6165	1.018	5483	1.016	5483	1.014	5204	1.011	4355	1	3766	0.99	3327	0.981	2984	0.974	1979	0.955	1190	0.932
2	4199	1.02	4018	1.019	3856	1.017	3710	1.015	3277	1.013	3141	1.005	2813	0.995	2553	0.987	2346	0.982	1168	0.965	1067	0.94
5	2008	1.02	1966	1.019	1926	1.018	1887	1.016	1851	1.014	1722	1.008	1613	1.003	1518	0.999	1436	0.995	1140	0.975	950	0.945

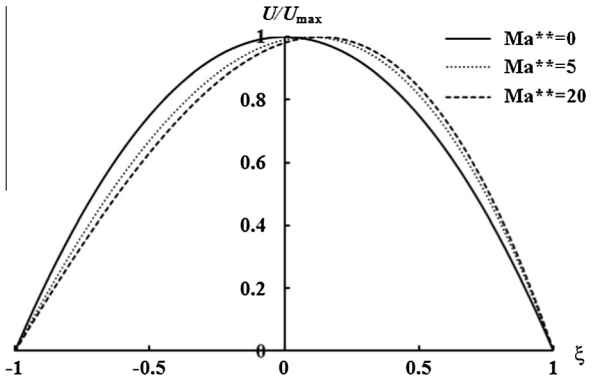

Fig. 3. Velocity profile in film at $Ca^{-1} = 1$. 1 – $Ma^{**} = 0$, 2–5, 3–20.

Thus one can conclude that the increase in the surface tension destabilizes the liquid film. A similar trend was also revealed theoretically in [9], where asymptotic solutions of different orders were investigated for the liquid film flow.

In the case where the surface tension depends on the temperature for $Ca^{-1} > 0$ and $Ma^{**} > 0$, the undisturbed velocity profile is distorted. Increasing the parameter Ca^{-1} leads to increasing the amplitude (maximum) velocity, and the growth of the parameter Ma^{**} causes both the increase in the amplitude and the offset of the maximum velocity (see Fig. 3) to the outer edge of the film. In this figure, U_{max} is the maximal value of the unperturbed velocity. As shown above, the increase in the amplitude of the unperturbed velocity entails the destabilization of the flow. Therefore, the simultaneous increase in both parameters Ca^{-1} and Ma^{**} causes the more rapid decrease in the critical Reynolds number (see Figs. 2 and 4 and Table 1). Besides, the increase in the parameter Ma^{**} under condition of Ca^{-1} = idem is accompanied with the decrease in the critical wavenumber (Fig. 5). Consequently, the increase in the temperature dependence of the surface tension causes the flow destabilization and makes the long-wavelength disturbances more dangerous.

An analysis of the structure of the Marangoni number leads to the conclusion that, in addition to the amplification of the temperature dependence of the surface tension (γ), the flow also is destabilized by the increase in the temperature difference (ΔT) and the decrease in the absolute pressure (increase Δh). The nature of the influence of temperature difference is obvious, as it reflects the effects of the Rayleigh–Bénard insatiability. The pressure reduction obviously causes the reduction in hydraulic resistance accompanied with the onset and amplification of the hydrodynamic instability. The increase in the thermal conductivity results in the stronger uniformity of the temperature field and thereby weakens the effects of the Rayleigh–Bénard instability. Therefore, the increase in the thermal conductivity, with the other parameters in the Marangoni number being constant, causes the stabilization of the flow.

To qualitatively validate the physical model used in the instability study, we have performed unsteady numerical simulations of capillary flow and heat transfer using ANSYS Fluent software. The simulation has been carried out in a two-dimensional rectangular computational domain of the size of $1 \cdot 10^{-5} \times 5 \cdot 10^{-4}$ m (Fig. 6). A two-phase VOF-model (Volume of Fluid method) [37] designed to solve the problems with the phase interface was applied for simulations. The following boundary conditions were used (Fig. 6):

(1) face 1: a water inlet at with atmospheric pressure and temperature set up (pressure-inlet);
(2) face 2: an adiabatic wall with non-slip velocity conditions;

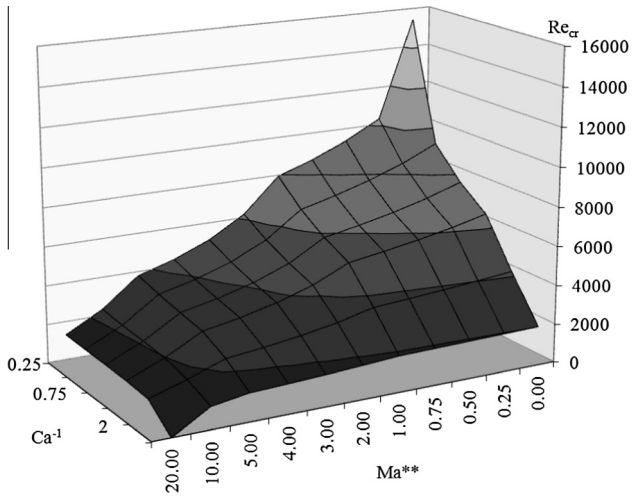

Fig. 4. Critical value of Reynolds number as function of cavity and number Marangoni number.

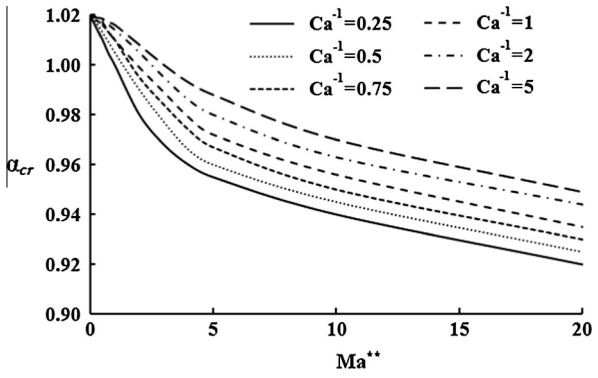

Fig. 5. Critical wavenumber vs Ma** at Ca^{-1} = idem.

(3) face 3: a wall with the temperature T_w and non-slip velocity conditions;
(4) face 4: a boundary between the phases with the specified surface tension as implemented in the model;
(5) face 5: pressure-outlet water with the specified atmospheric pressure and temperature;
(6) face 6: pressure-outlet vapor with the specified atmospheric pressure and temperature;
(7) face 7: an outflow, zero derivative of the velocity.

Fig. 6 depicts the configuration of the two-phase medium "water–vapor" at the initial moment of time. To perform a grid-independence study, three sizes of the grids have been validated in the simulations: a coarse grid with the discretization size of $1.0 \cdot 10^{-6}$, a fine grid with the discretization size of 2.5×10^{-7} m, and a very fine grid with the discretization size of 1.0×10^{-7}. The grid sized were 4400 cells, 70,400 cells and 440,000 cells, respectively. The velocity and temperature distributions for the fine and very fine grids differed from each other by not more than 0.5%. Therefore, the fine grid has been chosen for all subsequent simulations. Convergence was reached, if the residuals were smaller than 10^{-6} for the continuity and momentum equations and 10^{-9} for the energy equation.

Simulations demonstrated that at small values of the temperature difference across the film $\Delta T < 1^{\circ}$, the liquid film developed steadily with no visible disturbances. For large values of $\Delta T > 2.4^{\circ}$, noticeable disturbances arose in the film (Fig. 7). These disturbances escalated with time and lead to the disruption of the film. The dynamics of the behavior of such a film in time is shown in Fig. 8.

Although direct comparisons of the numerical simulations with the theoretical data of the instability analysis performed above, since the parameters used in the instability model cannot be determined from the numerical simulations. However, qualitatively the results provided by the numerical simulations and the instability analysis agree fairly well. Indeed, both approaches suggest existence of the fluid flow regimes with the stable and unstable film

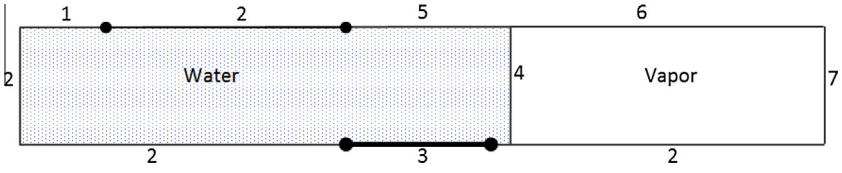

Fig. 6. A schematic of the computational domain.

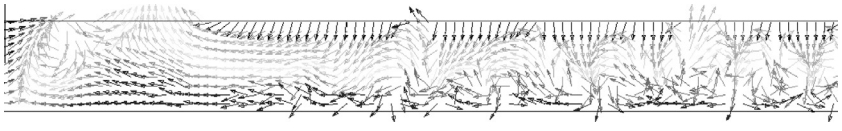

Fig. 7. Onset of the disturbances in the liquid film for $\Delta T > 2.4^{\circ}$.

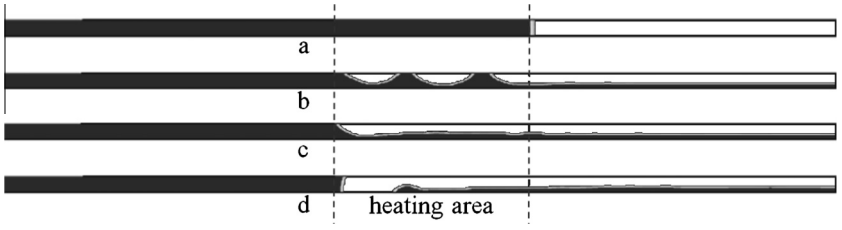

Fig. 8. Dynamics of the behavior of the liquid film in time for $\Delta T > 2.4^{\circ}$: (a) 0 s; (b) 9.5×10^{-6} s; (c) 3.75×10^{-4} s; (d) 4.205×10^{-4} s.

DOI : 10.1016/j.ijheatmasstransfer.2015.07.063

development depending on the temperature difference across the film.

Thus, in view of the applications in micro heat pipes, both the traditional instability and numerical CFD simulations enable undertaking an analysis to help estimate stability of the liquid film development.

8. Conclusions

The paper presents a novel 2D model for the thermocapillary instability of a thin liquid film. The model includes a novel solution for the unperturbed velocity components and the thin film thickness in the transition region subject to evaporation under the boundary conditions of (a) mechanical interaction between the liquid and vapor phases and (b) stationary vapor above the interphase boundary. The unperturbed velocity and temperature profiles for the basic flow were obtained in frames of the boundary layer approach. The expression for the film thickness was derived on the basis of the mass balance equation.

A novel model for the problem of the thermocapillary instability itself in a thin film was developed based on the linear perturbation method taking into account the surface and London–van der Waals forces. The unperturbed velocity profiles and the equation for the film thickness were used for the instability analysis performed using the modified Orr–Sommerfeld equation. The Squire's theorem, which was proved to be valid for the considered problem, has demonstrated that for the 2D flow the 2D disturbances are more dangerous than the three-dimensional disturbances. This is why the critical Reynolds number was computed by considering only the 2D disturbances.

The analysis of the results obtained based on the aforementioned novel model for the thermocapillary instability problem enabled elucidating the effects of the important non-dimensional parameters, such as the capillary number Ca and the modified Marangoni number Ma^{**}, on the critical Reynolds number.

For case of the constant surface tension independent of the temperature, i.e. at $Ca^{-1} > 0$ and $Ma^{**} = 0$, the unperturbed velocity profile exhibits a parabolic form. The increase in the parameter Ca^{-1} results in the increased value of the velocity at its maximum and does not affect the unperturbed velocity profile shape and the critical wave number $\alpha_{cr} = 1.02$, though causes the monotonic decrease in the critical Reynolds number.

For the case where the surface tension depends on the temperature ($Ca^{-1} > 0$ and $Ma^{**} > 0$), the maximum of the undisturbed velocity profile increases together with the parameters Ca^{-1} and Ma^{**}, whereas the increase in the parameter Ma^{**} shifts the maximum velocity towards the outer edge of the film. Simultaneously increasing parameters Ca^{-1} and Ma^{**} entail more rapid decrease in the critical Reynolds number, while the increase in the parameter Ma^{**} for the same value of Ca^{-1} is accompanied with the decrease in the critical wavenumber. Consequently, the increase in the temperature dependence of the surface tension causes the flow destabilization and makes the long-wavelength disturbances more dangerous.

It was also shown that the flow is destabilized by the increase in the temperature difference (ΔT), which reflects the effects of the Rayleigh–Bénard insatiability via the decrease in the absolute pressure (increase Δh), and subsequent reduction of the hydraulic resistance, the onset and amplification of the hydrodynamic instability. The increase in the thermal conductivity leads to weakening of the effects of the Rayleigh–Bénard instability.

Numerical simulations of the capillary flow and heat transfer have been performed using ANSYS Fluent software. The calculations demonstrated existence of the flow regimes with the stable and unstable film development depending on the temperature difference across the film. These results are qualitatively consistent with those suggested by the theoretical analysis of the flow instability.

Conflict of interest

None declared.

References

[1] F.L. Chang, Y.M. Hung, The coupled effects of working fluid and solid wall on thermal performance of micro heat pipes, Int. J. Heat Mass Transfer 73 (2014) 76–87.

[2] H. Shabgard, M.J. Allen, N. Sharifi, S.P. Benn, A. Faghri, T.L. Bergman, Heat pipe heat exchangers and heat sinks: opportunities, challenges, applications, analysis, and state of the art, Int. J. Heat Mass Transfer 89 (2015) 138–158.

[3] X. Liu, Y. Chen, Transient thermal performance analysis of micro heat pipes, Appl. Therm. Eng. 58 (2013) 585–593.

[4] Y.M. Hung, K.-K. Tio, Thermal analysis of optimally designed inclined micro heat pipes with axial solid wall conduction, Int. Commun. Heat Mass Transfer 39 (2012) 1146–1153.

[5] K.H. Do, S.P. Jang, Effect of nanofluids on the thermal performance of a flat micro heat pipe with a rectangular grooved wick, Int. J. Heat Mass Transfer 53 (2010) 2183–2192.

[6] L. Bammou, S. Blancher, Y. Le Guer, K. El Omari, B. Benhamou, Linear stability analysis of Poiseuille–Benard–Marangoni flow in a horizontal infinite liquid film, Int. Commun. Heat Mass Transfer 54 (2014) 126–131.

[7] Z. Ding, Q. Liu, Linear instability analysis of thermocapillary convection in a bilayer system, Int. J. Heat Mass Transfer 62 (2013) 63–72.

[8] I.I. Ryzhkov, V.M. Shevtsova, Thermocapillary instabilities in liquid columns under co – and counter-current gas flows, Int. J. Heat Mass Transfer 55 (2012) 1236–1245.

[9] A.M. Benselama, S. Harmand, K. Sefiane, A perturbation method for solving the micro-region heat transfer problem, Phys. Fluids 23 (10) (2011) 102103.

[10] A.M. Benselama, S. Harmand, K. Sefiane, Thermocapillary effects on steadily evaporating contact line: a perturbative local analysis, Phys. Fluids 24 (7) (2012) 072105.

[11] C. Ma, D. Bothe, Direct numerical simulation of thermocapillary flow based on the volume of fluid method, Int. J. Multiphase Flow 37 (2011) 1045–1058.

[12] Z. Zheng, L. Zhou, X. Du, Y. Yang, P. Jiang, B. Wang, Numerical investigation on Marangoni convection of binary fluids in a closed microcavity, Appl. Therm. Eng. (2014), http://dx.doi.org/10.1016/j.applthermaleng.2014.10.018.

[13] T. Gambaryan-Roisman, Modulation of Marangoni convection in liquid films, Adv. Colloid Interface Sci. (2015), http://dx.doi.org/10.1016/j.cis.2015.02.003.

[14] D.E. Melnikov, V.M. Shevtsova, The effect of ambient temperature on the stability of thermocapillary flow in liquid column, Int. J. Heat Mass Transfer 74 (2014) 185–195.

[15] D. Nezar, S. Rahal, Numerical simulation of convective instabilities in a liquid layer submitted to an inclined gradient of temperature, Energy Procedia 36 (2013) 380–385.

[16] Z. Pana, H. Wang, Benard–Marangoni instability on evaporating menisci in capillary channels, Int. J. Heat Mass Transfer 63 (2013) 239–248.

[17] I.B. Simanovskii, A. Viviani, F. Dubois, J.-C. Legros, Standing oscillations and traveling waves in systems with interfaces, Acta Astronaut. 97 (2014) 42–57.

[18] E.A. Chinnov, Wave-thermocapillary effects in heated liquid films at high Reynolds numbers, Int. J. Heat Mass Transfer 71 (2014) 106–116.

[19] B. Messmer, T. Lemee, K. Ikebukuro, I. Ueno, R. Narayanan, Confined thermocapillary flows in a double free-surface film with small Marangoni numbers, Int. J. Heat Mass Transfer 78 (2014) 1060–1067.

[20] J.-J. Yu, D.-F. Ruan, Y.-R. Li, J.-C. Chen, Experimental study on thermocapillary convection of binary mixture in a shallow annular pool with radial temperature gradient, Exp. Therm. Fluid Sci. 61 (2015) 79–86.

[21] P. Zhu, L. Duan, Q. Kang, Transition to chaos in thermocapillary convection, Int. J. Heat Mass Transfer 57 (2013) 457–464.

[22] L. Bammou, K. El Omaria, S. Blancher, Y. Le Guer, B. Benhamou, T. Mediouni, A numerical study of the longitudinal thermoconvective rolls in a mixed convection flow in a horizontal channel with a free surface, Int. J. Heat Fluid Flow 42 (2013) 265–277.

[23] R. Es Sakhy, K. El Omari, Y. Le Guer, S. Blancher, Rayleigh–Beynard–Marangoni convection in an open cylindrical container heated by a non-uniform flux, Int. J. Therm. Sci. 86 (2014) 198–209.

[24] E. Lim, Y.M. Hung, Thermocapillary flow in evaporating thin liquid films with long-wave evolution model, Int. J. Heat Mass Transfer 73 (2014) 849–858.

[25] J.R.A. Pearson, On convection cell induced by surface tension, J. Fluid Mech. 4 (1958) 489–500.

[26] W. Nusselt, Die Oberflächenkondensation des Wasserdampfes, Z. Ver. Deutsch. Ing. 60 (541–546) (1916) 569–575.

[27] C. Eberle, Versuche über den Warme- und Spannungsverlust bei der Fortleitung gesättigten und überhitzen Wasserdampfes, Z. Ver. Deutsch. Ing. (1908) 481.

[28] A.A. Avramenko, I.V. Shevchuk, A.I. Tyrinov, D.G. Blinov, Heat transfer at film condensation of moving vapor with nanoparticles over a flat surface, Int. J. Heat Mass Transfer 82 (2015) 316–324.
[29] A.A. Avramenko, I.V. Shevchuk, A.I. Tyrinov, D.G. Blinov, Heat transfer in stable film boiling of a nanofluid over a vertical surface, Int. J. Therm. Sci. 92 (2015) 106–118.
[30] M.E. Ellion, A study of the mechanism of boiling heat transfer, Jet Prop. Lab. Memo CIT 20 (1954) 1–88.
[31] J. Pretsch, Über die Stabilität einer Laminarströmung in einem geraden Rohr mit kreisförmigem Querschnitt, ZAMM 21 (1941) 204–217.
[32] H. Schlichting, A. Ulrich, Zur Berechnung des Umschlages laminar turbulent, Jahrbuch dt. Luftfahrtforsch. I (1942) 8–35.
[33] H.B. Squire, On the stability of three-dimensional disturbances of viscous fluid between parallel walls, Proc. R. Soc. London A 142 (1933) 621–628.
[34] C.A.J. Fletcher, Computational Galerkin Method, Spring-Verlag, New York, 1984. <http://www.maths.ox.ac.uk/chebfun/>.
[35] L.N. Trefethen, M. Embree, Spectra and Pseudospectra: The Behavior of Nonnormal Matrices and Operators, Princeton Univ Press, 2005.
[36] H. Schlichting, Boundary layer theory, seventh ed., McGraw-Hill, New York, 1979.
[37] C.W. Hirt, B.D. Nichols, Volume of fluid (VOF) method for the dynamics of free boundaries, J. Comput. Phys. 39 (1) (1981) 201–225.